Robustness Evaluation of Voltage and Current Model-Based Rotor Flux Estimation under Resistance Variations in FOC Systems

Vojtech Sotola[1], *Marek Kubatko*[1], *Quang Thanh Nguyen* [2,*], *Huy Duc Bui* [3], *Phung Hai Nguyen* [3]

[1]Department of Applied Electronics, Faculty of Electrical Engineering and Computer Science, VSB-Technical University of Ostrava, Ostrava, Czech Republic
[2]Power System Optimization Research Group, Faculty of Electrical and Electronics Engineering, Ton Duc Thang University, Ho Chi Minh City, Vietnam
[3]Faculty of Electrical and Electronics Engineering, Ton Duc Thang University, Ho Chi Minh City, Vietnam

Corresponding Author: [2,]Quang Thanh Nguyen (Email: nguyenthanhquang@tdtu.edu.vn)
Co-Authors: [1]Vojtech Sotola (Email: vojtech.sotola@vsb.cz), [1]Marek Kubatko (Email: marek.kubatko@vsb.cz), [3]Huy Duc Bui (Email: buiduchuy.st@tdtu.edu.vn), [3]Phung Hai Nguyen (Email: nguyenhaiphung.st@tdtu.edu.vn)
(Received: 03-April-2026; accepted: 11-June-2026; published: 30-June-2026)
http://dx.doi.org/10.55579/jaec.2026102.544

Abstract. *This study examines how two rotor flux estimators, the voltage model and the current model, behave when used within the same field-oriented control (FOC) structure for a three-phase induction motor drive. Particular attention is given to the effect of stator and rotor resistance variations, since these parameters directly enter the voltage and current model calculations and may change during operation due to heating. In the simulation study, both estimators are tested under low-, medium-, and high-speed conditions. A 30% increase in stator and rotor resistance is introduced while the drive is operating, and the resulting speed response and flux estimation behavior are then compared. The assessment is based on four time-domain error criteria: Integral of Absolute Error (IAE), Integral of Time multiplied Absolute Error (ITAE), Integral of Squared Error (ISE), and Integral of Time multiplied Squared Error (ITSE). The results show that the voltage model depends on the accuracy of the stator resistance, while the current model depends on the rotor resistance. This effect is most severe in the low-speed region, where the resistive voltage drop becomes significant relative to the applied stator voltage. At higher speeds, the voltage model error decreases, and the difference between the two estimators becomes smaller. These results indicate that the current model is a more reliable option when the drive is expected to operate under uncertainty in stator and rotor resistance, particularly at low speed.*

Keywords: *Current model, Voltage model, Rotor flux, Resistance variation, Field-oriented control.*

1. Introduction

Electric motors are widely used in modern industry, where they convert electrical energy into mechanical motion for use in production, transport, pumping, ventilation, and renewable en-

ergy, as well as robotics [1]. Among existing motor technologies, induction motors are still the most widely used today because of their robust construction and low maintenance requirements [2]. On the other hand, PMSM motors [3] and DC motors [4] remain the focus of research for applications that demand diverse high efficiency, miniaturization, or adjustable speed control.

Over the last few decades, various control strategies have been developed to address these challenges. Direct Torque Control (DTC) has emerged as a new approach that provides excellent torque response and a simple controller design [5, 6]. Although these advantages, DTC-based methods usually exhibit a high torque ripple and an inconsistent switching frequency, which deteriorate the steady-state performance [7]. The traditional V/f strategy is one of the simplest scalar control methods and relatively easy to implement [8]; however, it has weak disturbance rejection capability and poor dynamic performance [9,10]. Field-oriented control (FOC) remains a fundamental strategy for high-performance induction motor drives because it enables decoupled flux and torque regulation. Tran et al. [11] improved sensorless FOC by integrating stator-resistance estimation into CB-MRASCV. Nisha et al. [12] analyzed FOC under field-weakening operation, emphasizing torque capability in propulsion systems. Wolkiewicz et al. [13] showed that internal DFOC signals are valuable for early stator inter-turn fault monitoring. In addition to control performance, reliability has become a major concern in modern drive systems.

Sensor fault diagnosis in IMDs has increasingly shifted toward model-based comparison and signal reconstruction. Study in [14] used phase-shifted current space vectors to identify both soft and hard current sensor faults. Tran et al. [15] simplified FTC by comparing measured and estimated current vectors using a single observer. Publication [16] proposes fault-tolerant control (FTC) strategies to maintain stable operation under fault conditions, including sensor errors in speed and current. In sensorless FOC systems, accurate estimation of rotor flux is essential, and this has led to the development of two basic flux estimation methods: the voltage model (VM) and the current model (CM).

Several studies have employed the VM to estimate rotor flux and its orientation angle in induction motor drives. Hinkkanen and Luomi improved the conventional VM by replacing the pure integrator with a compensated low-pass structure, thereby reducing drift and improving behavior during speed reversal [17]. Brandstetter and Kuchar also underlined its simple application, although integration offset and stator resistance variation are still major challenges [18]. Similarly, Zamora et al. showed that estimation based on voltage and current can provide useful flux-related information, although its accuracy is constrained by parameter uncertainty, filtering requirements, and measurement noise [19].

Flux estimation based on CM has been widely investigated to improve field orientation in induction motor drives. The work in [20] discussed the design of a sliding-mode current model observer that needs less information about the rotor time constant and speed, and provides higher robustness for DFO control. Cuong et al. developed an MRAS in FOC and enhanced it with online stator and rotor resistance estimation, which improves its stability against thermal parameter variations [21]. Orlowska-Kowalska and Dybkowski showed that stator current-based MRAS (CB-MRAS) can provide stable wide-speed operation, although its performance remains affected by rotor parameter mismatches and by the selection of adaptation gains [22].

Recent MRAS-based studies have combined voltage and current models to improve sensorless induction motor control. Pal et al. modified RF-MRAS by replacing measured voltage with reference voltage to enhance low-speed estimation [23]. Research in [24] extended closed-loop MRAS to linear induction motors, accounting for end effects. In addition, publication [25] further improved regenerating-mode stability through a multilayer MRAS structure.

Parameter uncertainty is now well recognized as an important performance-degrading factor of field-oriented motor drive systems. Lazcano et al. emphasized that resistance variation can be leveraged for thermal monitoring,

but this requires accurate online estimation under realistic inverter nonidealities [26]. Publication [27] demonstrated that ignoring stator-resistance drift in FOC affects system efficiency. Similar issues can be found in MRAS-based sensorless drives that compensate stator resistance [28]. Yoo et al. have also shown that, especially at low speeds, it was necessary to design the resistance estimation schemes to avoid additional torque and flux ripples [29]. For RF-MRAS schemes, these observations imply that degradation in the voltage model branch under R_{st} variation may directly disturb the adaptation signal, especially at low speed.

This paper aims to provide a comprehensive review and comparative analysis of VM and CM for estimating rotor flux in the FOC framework when stator and rotor resistances vary. The study examines three realistic scenarios in which stator and rotor resistance increase due to thermal effects during operation. The impact of this variation on flux estimation accuracy and speed response is quantitatively evaluated using established performance indicators. Through this analysis, the paper seeks to clarify the relative stability of each model and provide practical insights into their applicability under parameter-sensitive operating conditions.

2. Methodology

2.1. Modeling a three-phase induction motor

The dynamic characteristics of an induction motor are modeled in the stationary (α–β) reference frame. The stator voltage equation can be expressed as:

$$\vec{u}_{st} = R_{st}\vec{i}_{st} + \frac{d\vec{F}_{st}}{dt} \tag{1}$$

where, $\vec{u}_{st}$ is the stator voltage vector (V), $\vec{i}_{st}$ is the stator current vector (A), R_{st} is the stator resistance (Ω), and $\vec{F}_{st}$ is the stator flux linkage vector (Wb).

The rotor circuit, assuming a squirrel-cage structure with no external voltage supply, is described by:

$$0 = R_{rt}\vec{i}_{rt} + \frac{d\vec{F}_{rt}}{dt} - j\omega_{rt}\vec{F}_{rt} \tag{2}$$

where, $\vec{i}_{rt}$ is the rotor current vector (A), R_{rt} is the rotor resistance (Ω), $\vec{F}_{rt}$ is the rotor flux linkage vector (Wb), and ω_{rt} is the rotor angular speed (rad/s), with:

$$\omega_{rt} = p\,\omega_m \tag{3}$$

where p is the number of pole pairs, and ω_m is the mechanical angular speed (rad/s).

The flux linkage relationships between stator and rotor circuits are given as:

$$\vec{F}_{st} = L_{st}\vec{i}_{st} + L_{mg}\vec{i}_{rt} \tag{4}$$

$$\vec{F}_{rt} = L_{mg}\vec{i}_{st} + L_{rt}\vec{i}_{rt} \tag{5}$$

where, L_{st} and L_{rt} are the stator and rotor inductances (H), respectively, and L_{mg} is the magnetizing inductance (H).

The electromagnetic torque is related to the load torque and rotor acceleration through the mechanical motion equation of the induction motor [30], as expressed below:

$$T_e = T_L + \frac{J_m}{p}\frac{d\omega_{rt}}{dt} \tag{6}$$

where, T_e is the electromagnetic torque (N·m), T_L is the load torque (N·m), and J_m is the moment of inertia (kg·m^2).

2.2. Rotor Flux Estimation Using the Voltage Model

In FOC schemes, the accurate estimation of rotor flux components is essential, as it directly determines the orientation of the rotating reference frame and, consequently, the overall control performance. Among the available approaches, the VM is widely adopted due to its

relatively simple structure and fast dynamic response. However, its accuracy is strongly influenced by parameter variations, particularly the stator resistance.

Based on the stator voltage equation in the stationary (α–β) reference frame, the rotor flux components can be reconstructed by integrating the difference between the stator voltage and the resistive voltage drop [31]. The estimated rotor flux components along the α and β axes are expressed as:

$$F_{rt,\alpha}^{V} = \frac{L_{rt}}{L_{mg}} \left[\int \left(u_{st,\alpha} - R_{st} i_{st,\alpha} \right) dt - \frac{L_{st} L_{rt} - L_{mg}^{2}}{L_{rt}} i_{st,\alpha} \right] \tag{7}$$

$$F_{rt,\beta}^{V} = \frac{L_{rt}}{L_{mg}} \left[\int \left(u_{st,\beta} - R_{st} i_{st,\beta} \right) dt - \frac{L_{st} L_{rt} - L_{mg}^{2}}{L_{rt}} i_{st,\beta} \right] \tag{8}$$

From these orthogonal components, the magnitude of the rotor flux vector is obtained as:

$$F_{rt}^{V} = \sqrt{\left(F_{rt,\alpha}^{V}\right)^{2} + \left(F_{rt,\beta}^{V}\right)^{2}} \tag{9}$$

The rotor flux angle, which is a critical variable for coordinate transformation in FOC, is determined by:

$$\theta_{F_{rt}}^{V} = \arctan\left(\frac{F_{rt,\beta}^{V}}{F_{rt,\alpha}^{V}} \right) \tag{10}$$

Where,

- $F_{rt,\alpha}^{V}$, $F_{rt,\beta}^{V}$: Rotor flux components estimated by the VM (Wb).
- F_{rt}^{V}: Magnitude of the rotor flux vector estimated by the VM (Wb).
- $\theta_{F_{rt}}^{V}$: Rotor flux angle estimated by the VM (rad).
- $u_{st,\alpha}$, $u_{st,\beta}$: Stator voltage components (V).
- $i_{st,\alpha}$, $i_{st,\beta}$: Stator current components (A).

In the VM approach, the stator resistance R_{st} directly affects the rotor flux calculation. This parameter is rarely constant in real drive systems, since winding temperature, loading condition, and operating duration can gradually change its value. When the resistance used in the estimator no longer matches the actual machine resistance, an error is introduced into the computed flux. This effect becomes more pronounced at low speeds, where the voltage drop across R_{st} accounts for a significant portion of the stator voltage. Consequently, both the estimated rotor flux magnitude and its angular position may deviate from their actual values. This sensitivity to R_{st} variation is therefore a key weakness of the voltage model. It provides a clear basis for comparing it with the current-model estimator, which does not rely directly on the stator resistance.

Figure 1 illustrates the FOC structure using the voltage model for rotor flux estimation. The DC-link voltage V_{DC} supplies a three-phase voltage source inverter, whose six semiconductor switches are gated by the sine PWM block to generate the motor phase voltages. The measured currents i_a, i_b, and i_c are transformed into the stationary components $i_{st,\alpha}$ and $i_{st,\beta}$, and also into the rotating components i_d and i_q. The voltage calculation block reconstructs $u_{st,\alpha}$ and $u_{st,\beta}$ from the inverter states and V_{DC}. These voltage and current components are then used by the voltage model to estimate the rotor flux F_{rt}^{V} and its angle $\theta_{F_{rt}}^{V}$.

The flux loop compares F_{ref} with F_{rt}^{V} to produce i_d^*, while the speed loop compares ω_{ref} with ω_{est} to generate i_q^*. The current PI controllers finally determine u_d and u_q, closing the control loop.

2.3. Rotor Flux Estimation Using the Current Model

Compared to the VM, which is defined by its integration of a continuously available dynamic quantity (rotor dynamics rather than direct volt-

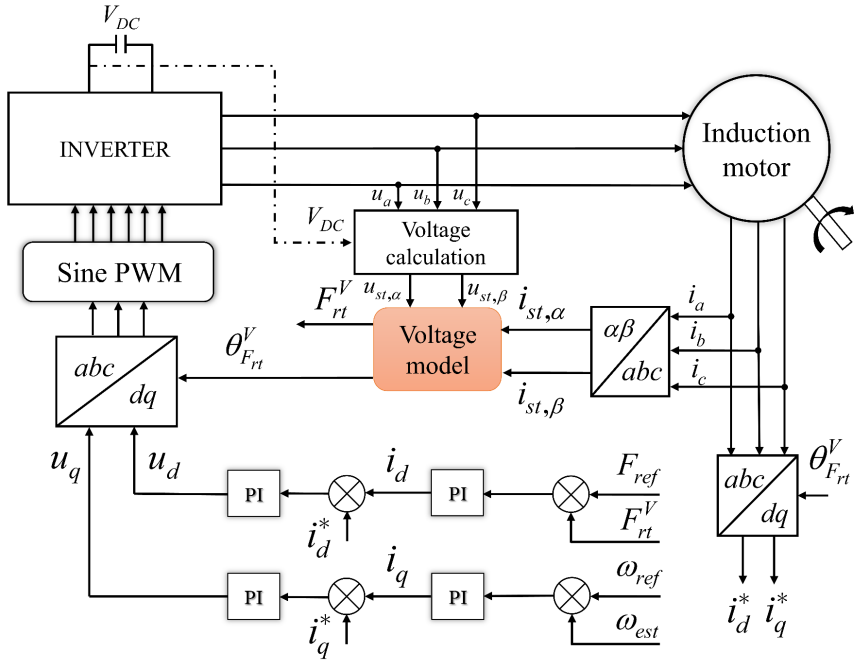

Figure 1: FOC scheme based on VM for rotor flux estimation.

age), the CM also offers an alternative formulation for rotor flux estimation. Such an approach is well suited to low-speed operation, where the VM is prone to drift and parameter sensitivity.

Starting from the rotor circuit equation and flux linkage relationships, the rotor flux dynamics in the stationary reference frame can be expressed as a first-order differential system. The estimated rotor flux components are obtained as [31]:

$$\frac{dF_{rt,\alpha}^I}{dt} = \frac{L_{mg}}{T_{rt}} i_{st,\alpha} - \frac{1}{T_{rt}} F_{rt,\alpha}^I + \omega_{rt} F_{rt,\beta}^I \quad (11)$$

$$\frac{dF_{rt,\beta}^I}{dt} = \frac{L_{mg}}{T_{rt}} i_{st,\beta} - \frac{1}{T_{rt}} F_{rt,\beta}^I - \omega_{rt} F_{rt,\alpha}^I \quad (12)$$

With

$$T_{rt} = \frac{L_{rt}}{R_{rt}} \quad (13)$$

where T_{rt} denotes the rotor time constant.

From these components, the magnitude of the rotor flux vector is computed as:

$$F_{rt}^I = \sqrt{\left(F_{rt,\alpha}^I\right)^2 + \left(F_{rt,\beta}^I\right)^2} \quad (14)$$

Similarly, the rotor flux angle required for coordinate transformation in the FOC scheme is obtained by:

$$\theta_{F_{rt}}^I = \arctan\left(\frac{F_{rt,\beta}^I}{F_{rt,\alpha}^I}\right) \quad (15)$$

Where,

- $F_{rt,\alpha}^I$, $F_{rt,\beta}^I$: Rotor flux components estimated by the CM (Wb).
- F_{rt}^I: Magnitude of the rotor flux vector estimated by the CM (Wb).
- $\theta_{F_{rt}}^I$: Rotor flux angle estimated by the CM (rad).

In the current model, rotor flux estimation is not directly affected by the stator resistance R_{st}.

This feature makes the method less vulnerable to errors associated with stator winding temperature rise, especially when compared with the voltage model. Its accuracy, however, is closely linked to the rotor circuit parameters. In particular, the rotor resistance R_{rt} appears through the rotor time constant T_{rt}, which governs the transient build-up and decay of the estimated rotor flux. During practical operation, R_{rt} also varies due to rotor heating. If the value used in the estimator differs from the actual rotor resistance, the computed rotor time constant becomes inaccurate. This mismatch can distort the estimated flux magnitude and shift the calculated rotor flux angle, thereby weakening the field orientation.

The CM depends strongly on the accuracy of R_{rt} and the availability of reliable rotor speed information. Figure 2 presents the FOC scheme in which the rotor flux is obtained from the current model. The DC source V_{DC} feeds a three phase inverter composed of six semiconductor switches, and the sine PWM unit assigns their gating signals to synthesize the stator voltages applied to the induction motor. The measured phase currents i_a, i_b and i_c are transformed into $i_{st,\alpha}$ and $i_{st,\beta}$, which, together with the rotor electrical speed ω_{rt}, serve as the inputs of the current model. This estimator provides the rotor flux magnitude F_{rt}^I and its position $\theta_{F_{rt}}^I$. The same angle is used in the abc/dq transformations to obtain i_d, i_q, i_d^*, and i_q^*. The flux regulator compares F_{ref} with F_{rt}^I, while the speed regulator compares ω_{ref} with ω_m. The resulting u_d and u_q are finally converted back to inverter commands. Compared with the voltage model, this structure avoids direct dependence on R_{st}, but its estimation quality remains governed by the rotor time constant and, consequently, by the variation of R_{rt}.

2.4. Quantitative Performance Evaluation

To evaluate the performance of the estimation methods, several time-domain performance indices are employed. These indices are computed from the speed tracking error between the reference speed and the actual motor speed. The speed tracking error is defined as:

$$e(t) = n_{ref}(t) - n_m(t) \tag{16}$$

where n_{ref} denotes the reference speed, and n_m denotes the actual motor speed.

The performance evaluation is carried out using four commonly used time-domain criteria: Integral of Absolute Error (IAE), Integral of Time multiplied Absolute Error (ITAE), Integral of Squared Error (ISE), and Integral of Time multiplied Squared Error (ITSE). The IAE index reflects the total accumulated tracking error during the evaluation interval. The ITAE index further emphasizes errors that persist for a longer time, making it suitable for assessing settling behavior. The ISE index gives greater weight to large transient errors due to the squared error term. Meanwhile, the ITSE index combines the effects of error magnitude and time duration, thereby highlighting large and sustained deviations in the speed response. The four evaluation indices are defined as follows:

1) Integral of Absolute Error (IAE)

$$IAE = \int_0^T |e(t)|dt \tag{17}$$

2) Integral of Time Multiplied Absolute Error (ITAE)

$$ITAE = \int_0^T t\,|e(t)|dt \tag{18}$$

3) Integral of Squared Error (ISE)

$$ISE = \int_0^T e^2(t)\,dt \tag{19}$$

4) Integral of Time Multiplied Squared Error (ITSE)

$$ITSE = \int_0^T t\,e^2(t)\,dt \tag{20}$$

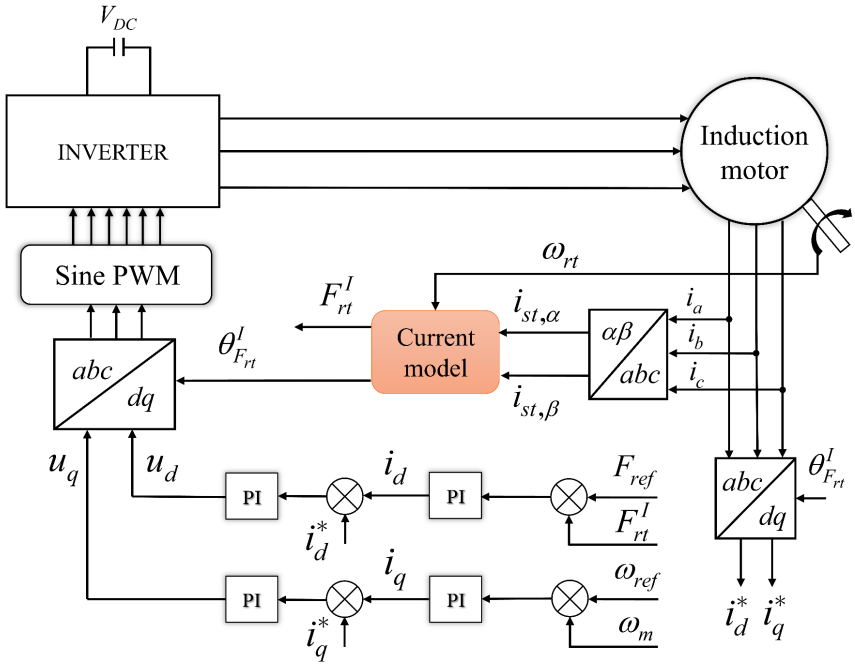

Figure 2: FOC scheme based on CM for rotor flux estimation.

where T denotes the total evaluation time of each simulation scenario.

IAE, ITAE, ISE, and ITSE capture both transient and steady-state performance, with time-weighted terms that emphasize long-lasting errors. These indices are used to assess accumulated error, long-duration deviation, large transient peaks, and sustained oscillatory errors, respectively. Simulations are conducted under varying R_{st} and R_{rt} resistances.

The angular speed deviation is defined as:

$$\Delta\omega_m(t) = \omega_{ref}(t) - \omega_m(t) \tag{21}$$

where ω_{ref} is the reference angular speed (rad/s).

3. Simulation and results

The simulation study was conducted using the induction motor parameters summarized in Table 1. The selected motor nameplate data are inherited from a previous study [27], thereby maintaining consistency with earlier research conditions. This also provides a common benchmark for future comparison of rotor flux estimation methods under parameter variations.

Table 1: Catalog of the Induction Motor.

Parameter	Value	Unit
Rated power P_n	2.2	kW
Rated frequency f_n	50	Hz
Rated speed n_{rated}	1420	rpm
Stator/Rotor resistance R_{st}/R_{rt}	3.179/2.118	Ω
Stator/Rotor inductance L_{st}/L_{rt}	0.209/0.209	H
Magnetizing inductance L_{mg}	0.192	H

3.1. Scenario 1: Low-Speed Operation (200 rpm)

The goal of this scenario is to analyze the effectiveness of the VM and CM at low speeds. Figures 3 – 7 illustrate the dynamic performance of the drive system under low-speed operation

with a step increase of 30% in both stator and rotor resistances at $t = 2$ s.

The simulation scenario assumes that the stator and rotor resistances simultaneously increase by 30% at the 2nd second (Figure 3). Figure 4 shows the motor's speed response tracking the reference speed. Before the stator and rotor resistances change, the system operates stably with good output speed quality. However, as the resistance increases, the motor speed in the VM case fluctuates more significantly than in the CM case. The deviation of motor speed is more clearly shown in Figure 5. In addition, the current in the dq coordinate system is also affected if the magnetic flux is not calculated accurately (Figure 6). Because, according to the Park transformation, the formula in this transformation includes the rotor flux angle, this will directly affect the accuracy of the current in the rotational coordinate system. Figure 7 directly represents the magnitude and angle of the rotor flux (in radians). In general, in low-speed operation mode, FOC control using a voltage model has weaker response performance than a current model when both stator and rotor resistances change simultaneously.

The sensitivity of the voltage model to stator resistance mismatch can be interpreted directly from its flux estimation equation. If the resistance used in the estimator is $\hat{R}_{st}$, while the actual resistance is R_{st}, the resulting resistance error is expressed as:

$$\Delta R_{st} = R_{st} - \hat{R}_{st} \tag{22}$$

The error introduces an additional voltage error term $-\Delta R_{st} i_{st}$ into the integrator. Therefore, the induced flux estimation error can be approximated as:

$$\Delta F_{rt}^{V} \approx -\int \Delta R_{st} i_{st}\, dt \tag{23}$$

Under sinusoidal steady-state operation, the magnitude of this error is approximately proportional to:

$$\left|\Delta F_{rt}^{V}\right| \propto \frac{|\Delta R_{st}|\,|i_{st}|}{\omega_s} \tag{24}$$

where ω_s is the synchronous angular speed (rad/s). This relationship indicates that the voltage model sensitivity increases as the stator frequency decreases. Consequently, at low speed, where the back-EMF is small and the resistive voltage drop becomes relatively dominant, even a moderate error in R_{st} can cause significant deviation in both rotor flux magnitude and angle.

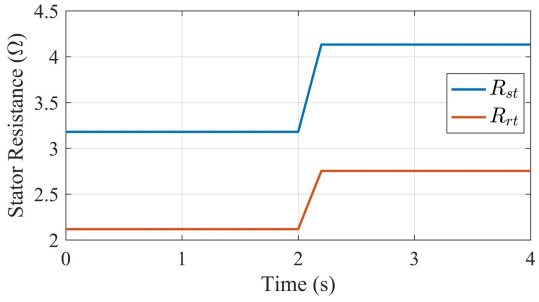

Figure 3: The simulation results of scenario 1: Resistance variation.

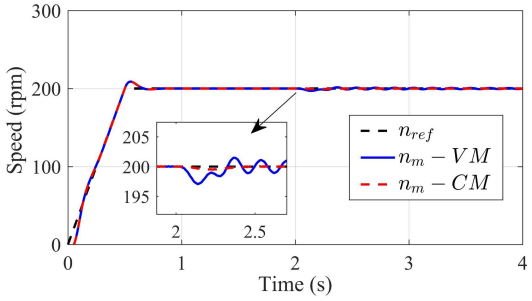

Figure 4: The simulation results of scenario 1: Speed responses.

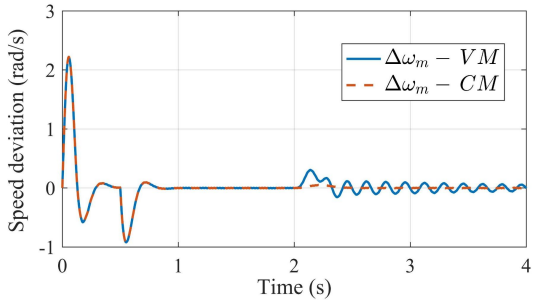

Figure 5: The simulation results of scenario 1: Speed deviations.

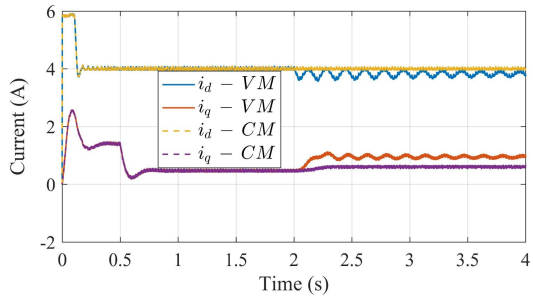

Figure 6: The simulation results of scenario 1: Currents in dq frame.

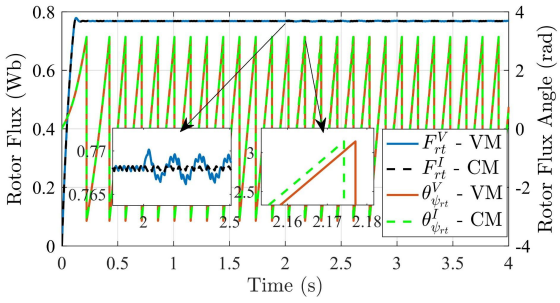

Figure 7: The simulation results of scenario 1: Magnitude & angle of rotor flux.

3.2. Scenario 2: Medium-Speed Operation (500 rpm)

Figures 8 – 12 present the simulation results of the drive system under medium-speed operation at 500 rpm, with a 30% increase in stator and rotor resistances applied at $t = 2$ s. As depicted in Figure 8, both resistances change abruptly to emulate the thermal drift that may occur during practical operation.

For medium-speed operation, the motor speed using the VM and the CM did not differ significantly from scenario 1 (Figure 9). At $t = 2$ s, when the resistances (R_{st} and R_{rt}) changed (Figure 8), the motor speed using the voltage model dropped to approximately 499 rpm, while the current model showed less fluctuation. It can be seen that the FOC drive system using the voltage model to calculate the rotor flux and flux angle still showed a weaker response than the case using the current model. The speed deviation at medium speed was more stable than at low speed (Figure 10).

The current components in the rotating reference frame are shown in Figure 11. Before changing the resistance, the i_d and i_q responses of both models were almost identical. After increasing R_{st} and R_{rt}, only small fluctuations in control were observed based on the voltage and current models. This confirms that both methods can maintain acceptable current regulation at this operating point, although the current model still offers slightly better stability. Figure 12 has two vertical axes: the left vertical axis represents the magnitude of the rotor flux, and the right vertical axis represents the angle of the rotor flux (from $-\pi$ to π).

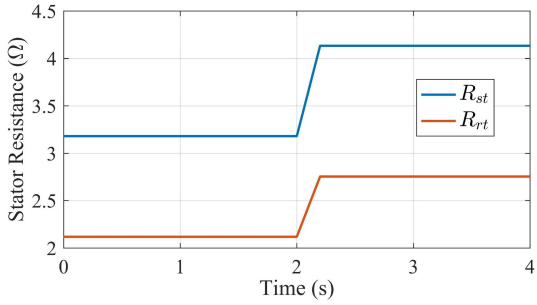

Figure 8: The simulation results of scenario 2: Resistance variation.

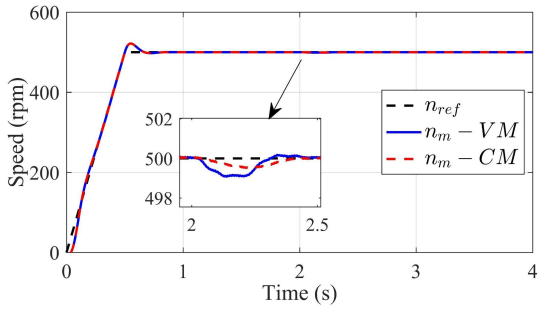

Figure 9: The simulation results of scenario 2: Speed responses.

3.3. Scenario 3: High-Speed Operation (900 rpm)

As illustrated in Figure 13, the change in resistance is identical to that in the previous scenarios, allowing consistent comparisons across different operating points. The speed response

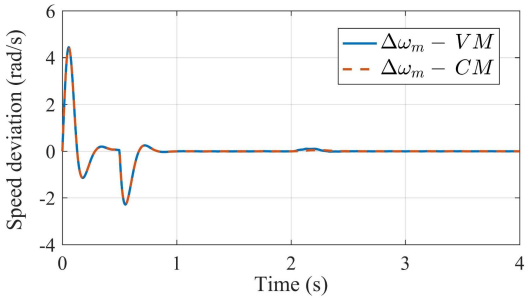

Figure 10: The simulation results of scenario 2: Speed deviations.

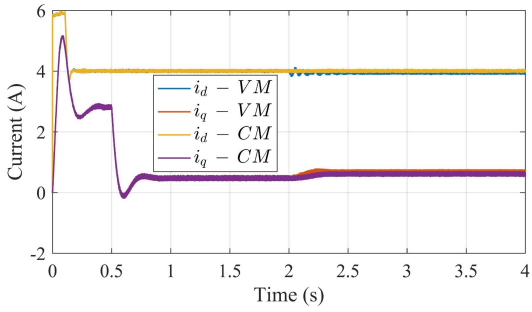

Figure 11: The simulation results of scenario 2: Currents in dq frame.

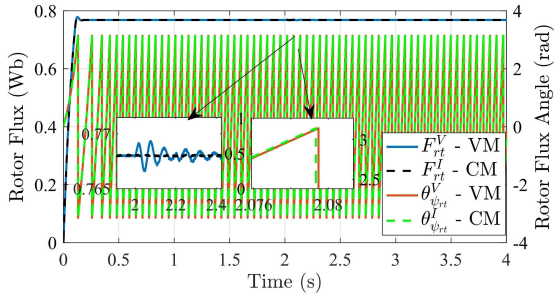

Figure 12: The simulation results of scenario 2: Magnitude & angle of rotor flux.

shown in Figure 14 indicates that both the voltage and current models achieve nearly identical performance. The transient response at $t = 2\,\mathrm{s}$ shows a small overshoot. This observation is further confirmed in Figure 15, where the speed deviation remains extremely small after $t = 2\,\mathrm{s}$ for both methods. The difference between the two estimation methods becomes negligible, with only slight high-frequency oscillations appearing in the voltage model. These oscillations have very low amplitudes and do not significantly affect the overall performance. The current responses in Figure 16 also show a high degree of similarity between the two models. Both the i_d and i_q components are stable before and after the change in resistance. Figure 17 directly represents the magnitude and angle of the rotor flux. At high operating speeds, the impact of changes in stator and rotor resistance on the voltage and current models becomes negligible. Therefore, both estimation methods yield comparable performance.

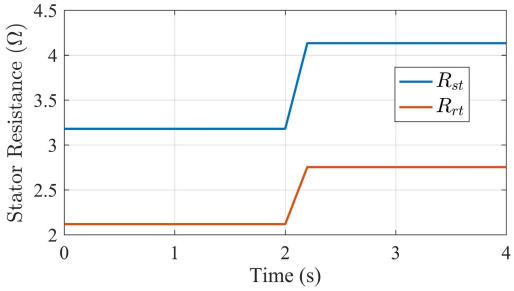

Figure 13: The simulation results of scenario 3: Resistance variation.

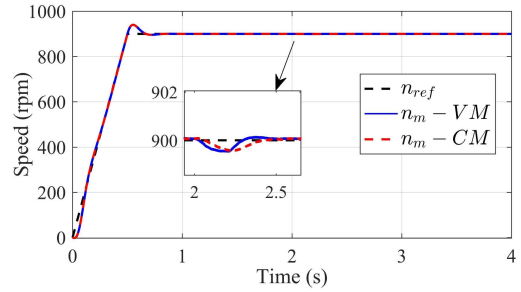

Figure 14: The simulation results of scenario 3: Speed responses.

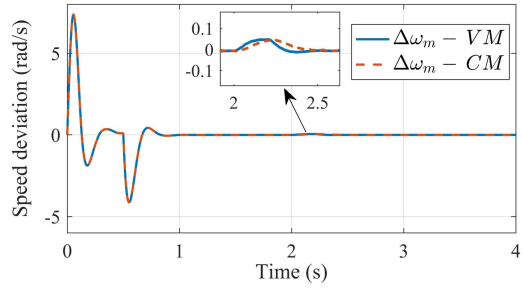

Figure 15: The simulation results of scenario 3: Speed deviations.

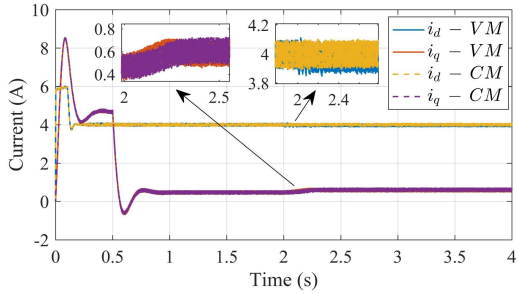

Figure 16: The simulation results of scenario 3: Currents in dq frame.

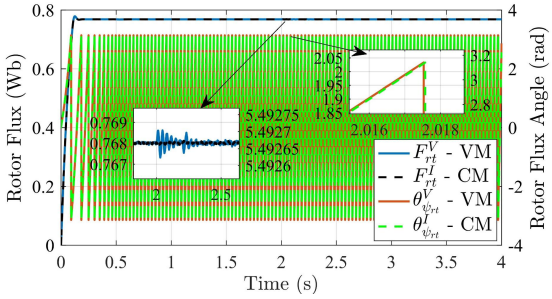

Figure 17: The simulation results of scenario 3: Magnitude & angle of rotor flux.

3.4. Discussion

Quantitative results provide clearer evidence of the differences in performance between the voltage and current models. At 200 rpm, the voltage model showed significantly larger errors in all four parameters: IAE = 1.4190, ITAE = 3.8750, ISE = 1.6310, and ITSE = 4.0490. In contrast, the corresponding values obtained with the current model were only IAE = 0.1594, ITAE = 0.3699, ISE = 0.0403, and ITSE = 0.0904. Thus, at low speeds, the voltage model error was approximately 10 times greater for IAE and ITAE, and more than 40 times greater for ISE and ITSE. This confirms that the voltage model is strongly affected at low speeds.

As speed increases, the performance of the voltage model improves significantly. For example, the VM-based IAE index decreases from 1.4190 at 200 rpm to 0.4939 at 300 rpm, 0.3158 at 400 rpm, and approximately 0.2696 at 900 rpm (Figure 18). A similar trend is observed in the ITAE, decreasing from 3.8750 to 0.6339 within the same speed range (Figure 19). The squared error indices show an even sharper decrease. ISE decreases from 1.6310 to 0.04465 (Figure 20), while ITSE decreases from 4.0490 to 0.09904 (Figure 21).

In comparison, the current model shows a much smoother variation. Its IAE index ranged from 0.1594 to 0.2603, and the ITAE index increased gradually from 0.3699 to 0.6161. The ISE and ITSE values remained almost constant, mostly in the 0.04–0.09 range. Overall, the current model provided more stable estimation quality as resistance varied.

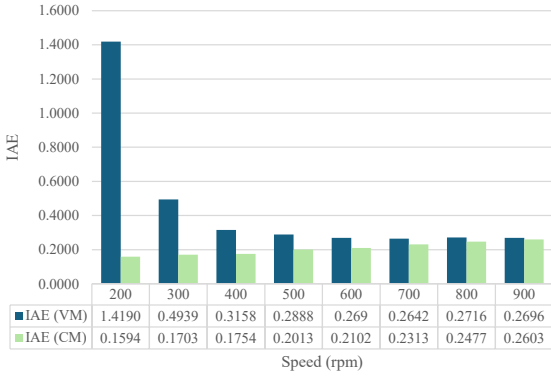

	200	300	400	500	600	700	800	900
IAE (VM)	1.4190	0.4939	0.3158	0.2888	0.269	0.2642	0.2716	0.2696
IAE (CM)	0.1594	0.1703	0.1754	0.2013	0.2102	0.2313	0.2477	0.2603

Figure 18: Quantitative evaluation based on IAE index.

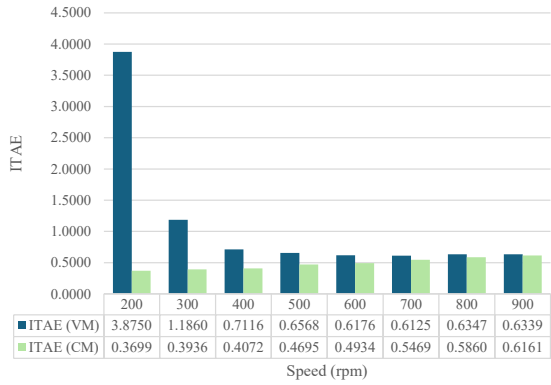

	200	300	400	500	600	700	800	900
ITAE (VM)	3.8750	1.1860	0.7116	0.6568	0.6176	0.6125	0.6347	0.6339
ITAE (CM)	0.3699	0.3936	0.4072	0.4695	0.4934	0.5469	0.5860	0.6161

Figure 19: Quantitative evaluation based on ITAE index.

4. Conclusion

This study presents an evaluation analysis comparing voltage and current models in esti-

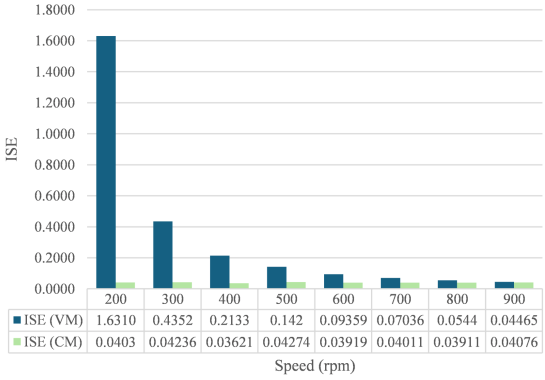

Figure 20: Quantitative evaluation based on ISE index.

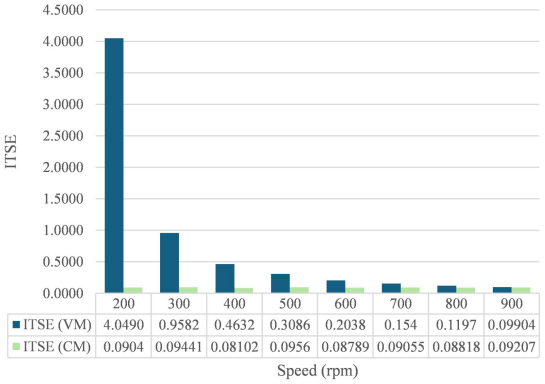

Figure 21: Quantitative evaluation based on ITSE index.

mating rotor flux in FOC structures. The influence of stator and rotor resistance on the operating efficiency of the motor drive system is quantitatively analyzed through the IAE, ITAE, ISE, and ITSE indices. The results show that the voltage model is highly sensitive to variations in machine parameters, especially at low speeds. This leads to instability of rotor flux magnitude and angle, thereby causing oscillations in the motor's speed response. In addition, the current model shows slight oscillations when rotor resistance changes at low speeds, but its efficiency is still better than that of the voltage model. As operating speed increases, the efficiency difference between the two methods gradually decreases.

Overall, the current model consistently achieves better efficiency. These findings confirm that the current model is more suitable for applications requiring high accuracy and reliability under parameter variations, especially in low-speed operation. Although the results clearly compare the voltage and current models under simultaneous R_{st} and R_{rt} variations, this study is limited to simulation-based validation. Practical factors such as measurement noise, sampling delay, inverter dead time, voltage drop, and discretization errors may further affect flux magnitude and angle estimation. Therefore, future work will focus on real-time and experimental validation under hardware nonidealities.

Acknowledgement

The authors thank Ton Duc Thang University and VSB-Technical University of Ostrava for their support in this work.

References

[1] D. Zellouma, Y. Bekakra, and H. Benbouhenni. Field-oriented control based on parallel proportional–integral controllers of induction motor drive. *Energy Reports*, 9:4846–4860, 2023. DOI: 10.1016/j.egyr.2023.04.008

[2] A. Gundogdu, R. Celikel, B. Dandil, and F. Ata. FPGA in-the-loop implementation of direct torque control for induction motor. *Automatika*, 62(2):275–283, 2021. DOI: 10.1080/00051144.2021.1934365

[3] Y. Zhang, J. Jin, and L. Huang. Model-free predictive current control of PMSM drives based on extended state observer using ultralocal model. *IEEE Transactions on Industrial Electronics*, 68(2):993–1003, Feb. 2020. DOI: 10.1109/TIE.2020.2970660

[4] W. Kong, H. Zhang, X. Yang, Z. Yao, R. Wang, W. Yang, and J. Zhang. PID control algorithm based on multistrategy enhanced dung beetle optimizer and back propagation neural network for DC motor control. *Scientific Reports*, 14(1):28276, 2024. DOI: 10.1038/s41598-024-79653-z

[5] S. G. Malla. A review on Direct Torque Control (DTC) of induction motor: With applications of fuzzy. In *Proc. 2016 International Conference on Electrical, Electronics, and Optimization Techniques (ICEEOT)*, Chennai, India, pp. 4557–4567, 2016. DOI: 10.1109/ICEEOT.2016.7755579

[6] M. S. Zaky. High performance DTC of induction motor drives over a wide speed range. *Electrical Engineering*, 97(2):139–154, 2015. DOI: 10.1007/s00202-014-0321-2

[7] M. M. Amin, F. F. M. El-Sousy, O. A. Mohammed, G. A. Abdel Aziz, and K. Gaber. MRAS-based super-twisting sliding-mode estimator combined with block control and DTC of six-phase induction motor for ship propulsion application. *IEEE Transactions on Industry Applications*, 57(6):6646–6658, 2021. DOI: 10.1109/TIA.2021.3115088

[8] Y. N. Dementyev, N. V. Kojain, A. D. Bragin, and L. S. Udut. Control system with sinusoidal PWM three-phase inverter with a frequency scalar control of induction motor. In *Proc. 2015 International Siberian Conference on Control and Communications (SIBCON)*, Omsk, Russia, pp. 1–6, May 2015. DOI: 10.1109/SIBCON.2015.7147008

[9] H. A. Mohammed and A. N. B. Alsammak. An intelligent hybrid control system using ANFIS-optimization for scalar control of an induction motor. *Journal Européen Des Systèmes Automatisés*, 56(5):857, 2023. DOI: 10.18280/jesa.560516

[10] A. S. Abdel-Khalik, R. A. Hamdy, A. M. Massoud, and S. Ahmed. Postfault control of scalar (V/f) controlled asymmetrical six-phase induction machines. *IEEE Access*, 6:59211–59220, 2018. DOI: 10.1109/ACCESS.2018.2874133

[11] C. D. Tran, P. Brandstetter, M. Kuchar, and P. D. Nguyen. An improved CB-MRAS using voltage model integrating stator resistance estimation in induction motor drives. *International Review of Electrical Engineering (IREE)*, 19(6):446–452, 2024. DOI: 10.15866/iree.v19i6.25107

[12] G. K. Nisha, Z. V. Lakaparampil, and S. Ushakumari. Effect of power factor on torque capability of FOC induction machine in field weakening region for propulsion systems. *Electrical Engineering*, 99(3):1065–1072, Sep. 2017. DOI: 10.1007/s00202-016-0479-x

[13] M. Wołkiewicz, G. Tarchała, T. Orłowska-Kowalska, and C. T. Kowalski. Online stator interturn short circuits monitoring in the DFOC induction-motor drive. *IEEE Transactions on Industrial Electronics*, 63(4):2517–2528, Apr. 2016. DOI: 10.1109/TIE.2016.2520902

[14] Q. S. Vu, C. D. Tran, B. H. Dinh, C. S. T. Dong, H. T. Huynh, and H. X. Phan. A current sensor fault diagnosis method based on phase angle shift technique applying to induction motor drive. *International Journal of Power Electronics and Drive Systems (IJPEDS)*, 13(3):1315–1325, 2022. DOI: 10.11591/ijpeds.v13.i3

[15] C. D. Tran, P. Brandstetter, M. H. C. Nguyen, S. D. Ho, P. N. Pham, and B. H. Dinh. An enhanced fault tolerant control against current sensor failures in induction motor drive by applying space vector. *Journal of Advanced Engineering and Computation*, 4(1):51–63, 2020. DOI: 10.25073/jaec.202041.269

[16] C. D. Tran, M. Kuchar, V. Sotola, and P. D. Nguyen. Sensor fault diagnosis strategy based on rotor flux observers in three-phase induction motor drive. *Scientific Reports*, 16:267, 2026. DOI: 10.1038/s41598-025-29381-9

[17] M. Hinkkanen and J. Luomi. Modified integrator for voltage model flux estimation of induction motors. In *Proc. IECON'01: 27th Annual Conference of the IEEE Industrial Electronics Society*, Denver, CO, USA, 2:1339–1343, 2001.

[18] P. Brandstetter and M. Kuchar. Rotor flux estimation using voltage model of induction motor, In *Proc. 16th International Scientific Conference on Electric Power Engineering (EPE)*. Kouty nad

Desnou, Czech Republic, pp. 246–250, 2015. DOI: 10.1109/EPE.2015.7161090

[19] J. L. Zamora, A. Garcia-Cerrada, and A. Zazo. Rotor-speed estimator for induction motors using voltage and current measurements. *Control Engineering Practice*, 6(3):369–383, 1998. DOI: 10.1016/S0967-0661(97)00022-1

[20] H. U. Rehman, M. K. Gilven, A. Derdiyok, and L. Xu. A new current model flux observer insensitive to rotor time constant and rotor speed for DFO control of induction machine. In *Proc. IEEE 32nd Annual Power Electronics Specialists Conference (PESC)*, 2:1179–1184, Vancouver, BC, Canada, Jun. 2001. DOI: 10.1109/PESC.2001.954279

[21] D. C. Tran, T. T. Phan, Q. T. Nguyen, and K. D. T. Phan. Improved MRAS with stator and rotor resistance estimation for vector control of induction motors. *Journal of Military Science and Technology*, 109:14–24, 2026. DOI: 10.54939/1859-1043.j.mst.109.2026.14-24

[22] T. Orłowska-Kowalska and M. Dybkowski. Stator-current-based MRAS estimator for a wide range speed-sensorless induction-motor drive. *IEEE Transactions on Industrial Electronics*, 57(4):1296–1308, Apr. 2010. DOI: 10.1109/TIE.2009.2031134

[23] A. Pal, S. Das, and A. K. Chattopadhyay. An improved rotor flux space vector based MRAS for field-oriented control of induction motor drives. *IEEE Transactions on Power Electronics*, 33(6):5131–5141, Jun. 2017. DOI: 10.1109/TPEL.2017.2657648

[24] A. Accetta, M. Cirrincione, M. Pucci, and G. Vitale. Closed-loop MRAS speed observer for linear induction motor drives. *IEEE Transactions on Industry Applications*, 51(3):2279–2290, May/Jun. 2015. DOI: 10.1109/TIA.2014.2375377

[25] K. Wróbel, G. Tarchała, K. Szabat, and S. Katsura. Improving regenerating mode operation of MRAS-based induction motor speed estimation using the multilayer technique. *IEEE Access*, 12:153063–153073, 2024. DOI: 10.1109/ACCESS.2024.3481053

[26] U. Lazcano, J. Poza, F. Garramiola, C. A. Rivera, and I. Iturbe. Double Dead-Time Signal Injection Strategy for Stator Resistance Estimation of Induction Machines. *Applied Sciences*, 12(17):8812, 2022. DOI: 10.3390/app12178812

[27] C. D. Tran, M. Kuchar, and P. D. Nguyen. Improved speed sensorless control for induction motor drives using rotor flux angle estimation. *Electrical Engineering & Electromechanics*, 6:93–97, 2025. DOI: 10.20998/2074-272X.2025.6.12

[28] Y. A. Khan and V. Verma. Stator resistance estimation for MRAS-based speed sensorless vector-controlled switched reluctance motor drive. *Electrical Engineering*, 103(4):1949–1963, 2021. DOI: 10.1007/s00202-020-01203-3

[29] J. Yoo, J. Lee, S.-K. Sul, and N. A. Baloch. Stator resistance estimation using DC injection with reduced torque ripple in induction motor sensorless drives. *IEEE Transactions on Industry Applications*, 56(4):3744–3754, 2020. DOI: 10.1109/TIA.2020.2984189

[30] A. Devanshu, M. Singh, and N. Kumar. Artificial neural network-based current control of field oriented controlled induction motor drive. *Electrical Engineering*, 103:1093-1104, 2021. DOI: 10.1007/s00202-020-01138-9

[31] M. Diop, A. Kebe, and I. Gueye. Evaluation of sensorless VF-MRAS and FOC-MRAS of IM electrical drive system. *International Journal of Applied Power Engineering*, 14(3):513-521, 2025. DOI: 10.11591/ijape.v14.i3.pp513-521

About Authors

Vojtech Sotola was born in Karvina, Czech Republic, in 1995. He is currently an Academic Staff Member with the Faculty of Electrical Engineering and Computer Science, VSB-Technical University of Ostrava, Czech Republic. His main research interests include DSC-based control systems, sensorless and sensor fault-tolerant control of AC drives, and applications of observers, estimators, and soft computing methods in electrical drive control. He can be contacted at email: vojtech.sotola@vsb.cz.

Marek Kubatko was born in Bohumin, Czech Republic, in 1996. He is currently a researcher with the Faculty of Electrical Engineering and Computer Science, VSB-Technical University of Ostrava, Czech Republic. His main research interests include DSC-based control systems, sensorless and sensor fault-tolerant control of AC drives, and applications of ANN observers, estimators, and soft computing methods with ANN in electrical drive control. He can be contacted at email: marek.kubatko@vsb.cz.

Quang Thanh Nguyen was born in Vietnam in 1991. He received a Master's degree in Automation and Control Engineering from Ton Duc Thang University, Ho Chi Minh City, Vietnam, in 2019. Now, he is a Ph.D. candidate and lecturer specializing in Electrical Engineering, Faculty of Electrical and Electronics Engineering, Ton Duc Thang University, Vietnam. His research interests include microcontrollers, robots, SCADA, and intelligent algorithms in motor drives. He can be contacted at email: nguyenthanhquang@tdtu.edu.vn.

Huy Duc Bui received his Bachelor of Engineering degree in Electrical Engineering from Ton Duc Thang University, Ho Chi Minh City, Vietnam, in 2021. He is currently working as an Electrical Engineer. Now, he is a Master student in Electrical Engineering, Faculty of Electrical and Electronics Engineering, Ton Duc Thang University, Vietnam. He can be contacted at email: buiduchuy.st@tdtu.edu.vn.

Phung Hai Nguyen is the Director of Lin Ka Services Co. Ltd, Level 5, Songdo Building, 62A Pham Ngoc Thach Street, Vo Thi Sau Ward, Dist.3, HCM City, Vietnam. Now, he is a Master student in Electrical Engineering, Faculty of Electrical and Electronics Engineering, Ton Duc Thang University, Vietnam. He can be contacted at email: nguyenhaiphung.st@tdtu.edu.vn.